Scholars Journal of Engineering and Technology

OPEN ACCESS

Abbreviated Key Title: Sch J Eng Tech
ISSN 2347-9523 (Print) | ISSN 2321-435X (Online)
Journal homepage: https://saspublishers.com

Numerical Simulations of Shock Wave Turbulent Boundary Layer Interaction over a Flat Plate at Mach 6

R. C. Mehta[1*]

[1]Noorul Islam Centre for Higher Education, Kumaracoil 629180, India

DOI: https://doi.org/10.36347/sjet.2025.v13i01.006 | **Received:** 03.12.2024 | **Accepted:** 09.01.2025 | **Published:** 13.01.2025

***Corresponding author:** R. C. Mehta
Noorul Islam Centre for Higher Education, Kumaracoil 629180, India

Abstract | **Original Research Article**

Unsteady numerical simulation is carried out for shock wave turbulent boundary layer interaction (SWTBLI) at wedge shock angle $\theta_w = 10^o$ over a flat plate at freestream Mach 6 for freestream Reynolds number varying from 17.2×10^6, 37.3×10^6 and 72.8×10^6/m and wall to stagnation temperature ratio $T_w/T_\infty = 0.56$. A preliminary investigation is presented to analyse the fluid-surface interaction and to determine the sound pressure level. Spectral analysis is carried out using Fast Fourier Transform. The maximum shock wave frequency is about 645 Hz. The maximum sound pressure level of 110 dB is found near the separation points. The pressure and the heat flux fluctuations are found to be strongly, especially near the separation and reattachment points.

Keywords: CFD, Separated flow, Shock wave, Turbulent boundary layer, Unsteady flow, Hypersonic flow.

1. INTRODUCTION

The shock wave turbulent boundary layer interaction (SWBLI) is one of the challenging problems in high-speed aerodynamics. The complicated nature of the separated boundary layer, attributed to a shock wave interaction with boundary layer, having adverse pressure gradient generate fluctuating pressure and heat transfer loads over structure. This will alter flow topology of viscous-inviscid flow which yields a non-uniformity of the flow field. These shock wave boundary layer interaction problems are occurred in high-speed vehicles such as manoeuvring missile, scram jet engine, launch vehicle and propulsive rocket nozzle. The shocks induced boundary layer separation results loss of control effectiveness, loss of total pressure and drop in aerodynamic efficiency and can cause large scale fluctuations detrimental to vehicles. It is, therefore, essential to have in depth information of the flow field for efficient performance of the vehicles.

Hayashi, Aso and Tan [1] have measured fluctuating wall heat flux components in shock wave turbulent boundary layer interaction at $M_\infty = 4.0$, $T_w/T_\infty = 0.56$ and 0.57, $Re_L = 1.26 \times 10^7$, $\theta_w = 18.5^o$ and 22.3^o. They have measured significant fluctuations in wall heat flux throughout the SWTBLI region. However, strong surface pressures as well as wall heat flux fluctuations are observed in the vicinity of the separation and reattachment regions. Relationship between peak surface pressure and wall heat transfer coefficient is obtained at Mach 6. Spectral analysis of surface pressure and wall heat flux time history is presented using Fast Fourier Transform (FFT) for freestream Reynolds number of 72.8×10^6/m. The sound pressure level and corresponding frequencies for unsteady surface pressure oscillations are required to maintain structural integrity of space vehicle.

Survey and progress on the shock wave/turbulent boundary layer interaction research has been described in Refs. [2] and [3]. Physical aspects of the SWTBLI has been discussed by Delery *et al.*, [4]. Review of low-frequency unsteadiness of SWTBLI has been reviewed by Clemens *et al.*, [5]. Experimental and numerical studies have been carried out by Lu *et al.*, [6] to understand the physics of SWTBLI at $M_\infty = 3.4$, $Re = 6.30 \times 10^7$/m, $\theta_w = 15^o$. Tong *et al.*, [7] have studied turbulent heat flux and temperature variance in supersonic SWTBLI. Numerical simulation [8] shows a low-frequency unsteadiness at separation and a high-frequency at reattachment due to SWTBLI.

A schematic sketch of SWTBLI flow field over a flat plate is shown in Fig. 1 with incident wedge (oblique) shock angle θ_w. The boundary layer thickness ahead of the point of impinging of the oblique shock wave increases independent of whether separation occurs or not. The pressure increases at the outer edge of the

boundary layer corresponding to the curvature streamline in the direction of the flat plate and it separates the outer layer from the boundary layer. Influence of the expansion waves shows a mild fall in pressure in the boundary layer.

Main Focus of the present paper to numerically analysis the unsteady, compressible Reynolds-averaged Navier-Stokes (RANS) is carried out for shock wave/turbulent boundary layer interaction (SWTBLI) at oblique shock generator 10^o over a flat plate at Mach 6 for freestream Reynolds number varying from 17.2×10^6, 37.3×10^6 and 72.8×10^6/m and wall to total temperature ratio of 0.56. The present two-dimensional SWTBLI is ideal case for numerical as well as experimental data of wind tunnel studies. The present numerical analysis computes the mean and the fluctuating flow along the flat plate, range of sound pressure levels and fluctuations of heat flux and corresponding frequencies. The main aim of the present paper is to analyse spectrum analysis of time-dependent wall pressure and wall heat flux fluctuations using Fast Fourier Transform; and to study the primary mechanism for the generation of peak heating to linked with the turbulence amplification in the interaction region with wall pressure.

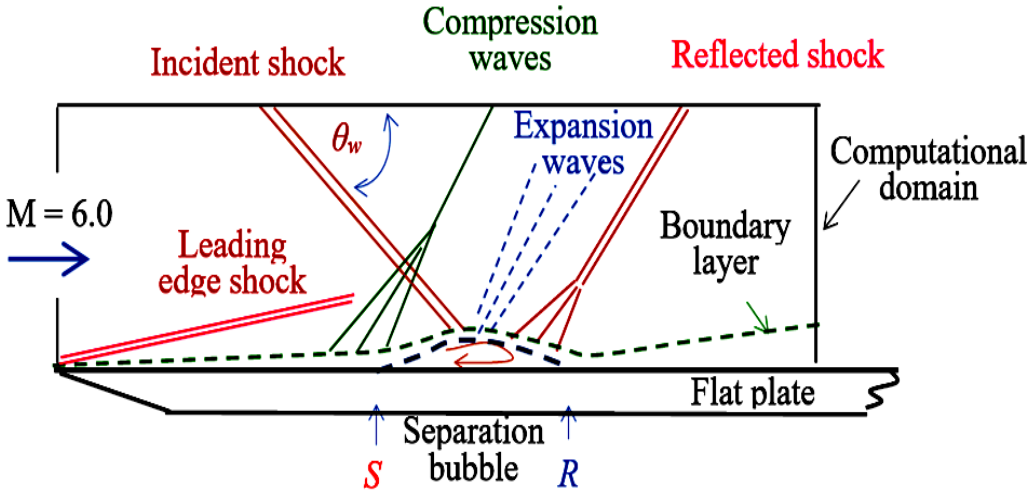

Fig 1: Schematic sketch of SWBLI flow field

2. NUMERICAL METHODS

MacCormack's implicit analogue [9] of unsplit explicit finite difference flow solver was employed to solve Reynolds-averaged Navier-Stokes (RANS) equations. The numerical scheme is second-order accurate in spatial and temporal domain. Baldwin-Lomax algebraic model [10] is used. A global time-step is used.

$$\Delta t = min\left[\frac{|u|}{\Delta x}+\frac{|v|}{\Delta y}+c\sqrt{\frac{1}{(\Delta x)^2+(\Delta y)^2}}\right]^{-1} \quad \ldots\ldots\ldots\ldots\ldots\ldots (1)$$

Where Δt is the time step. Δx and Δy are spatial increments in axial and normal directions respectively.

Initial and Boundary Conditions

Initial conditions are chosen as freestream values except the flow variables at the mesh boundary are set to values for a given shock strength so that the shock wave should impinge on the flat plate surfaces at the lower boundary at a given point. The initial flowfield and boundary conditions, interaction of the incident shock and the expansion fan originating from the oblique shock generator are shown schematically shown in Fig. 2. At the solid wall boundary, no-slip conditions are implemented and the wall is assumed to be isothermal. Table 1 shows flow conditions of wind tunnel [11].

Table 1: Flow conditions at $M_\infty = 6$ and $\theta_w = 10^0$

P_o, Pa	T_o, ^{0}K	T_w/T_o	Re/m	$Re_{x,s}$
2.2	528	0.56	17.2×10^6	5.44×10^6
4.9	533	0.56	37.3×10^6	11.14×10^6
9.8	540	0.56	72.8×10^6	20.68×10^6

A symmetric condition is applied ahead of the leading edge of the plate. Pressure is calculated at the centre of each cell. At the out-flow boundary, linear extrapolation is used for the conservative variables. At

the top boundary, flow conditions are adopted from an inviscid simulation at oblique shock generator of 10^0.

Flat Plate Geometry

The flat plate had width of 45.6 cm and span of 17.46 cm. The pressure plate had a constant wall thickness of 0.318 cm. The height of wedge leading above plate is a_w = 7.29 cm as shown in Fig 2. The wedge generator was 19.05 cm long and had a span of 15.24 cm. The wedge shock generator angle set 10^0. These dimensions are ideal two-dimensional case to numerically simulate shock wave/turbulent boundary layer interaction.

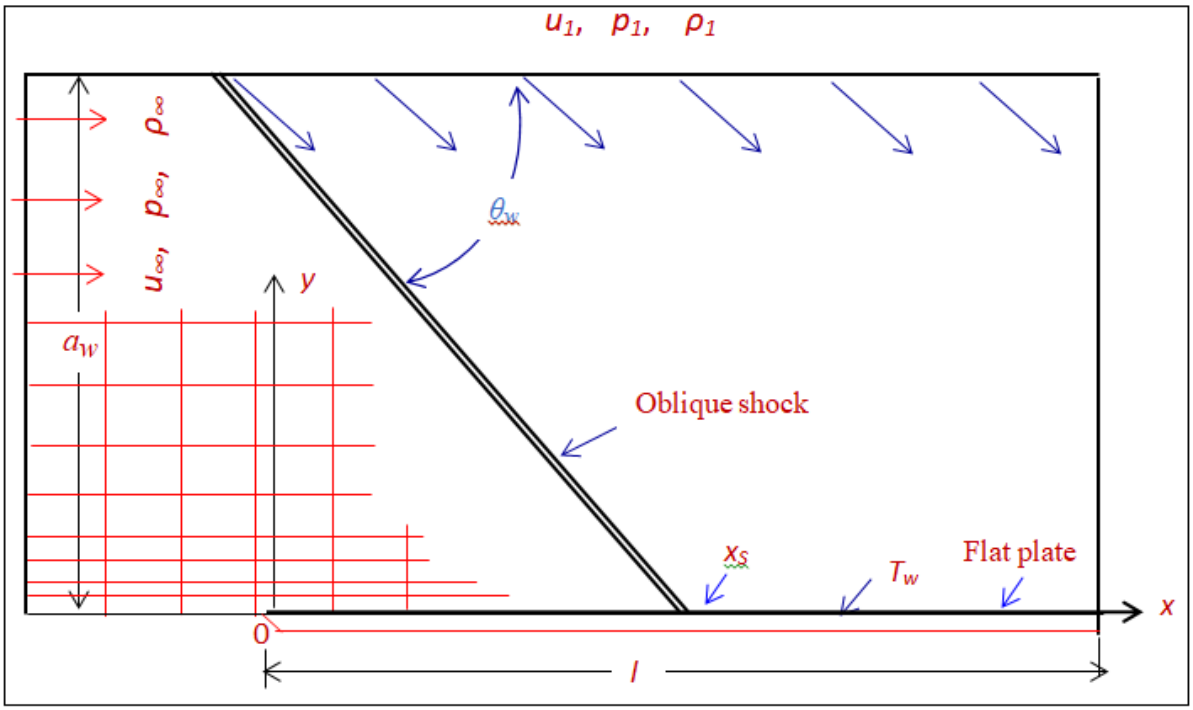

Fig 2: Initial conditions for shock wave/boundary layer interaction

Computational Grid

A grid independence check for the solution is performed employing different types of grid arrangement, such as 64 × 40, 72 × 32 and 82 × 42. Nearly identical solutions were obtained in all the cases. For correct representation of a turbulent boundary layer, at least one mesh point should appear in the laminar sub-layer. Physically, one mechanism for unsteadiness observed in supersonic separated flows is ascribed in pressure fluctuations at reattachment. The source of any such disturbances, should they be due to physical phenomena, must therefore be ascribed to attributes of the flow which the code can model.

3. RESULTS AND DISCUSSION

Data Processing

The computer used for the analysis was workstations. The data processing rate defined here as CPU time/ grid point/iteration time is about 1.85 $\times 10^{-9}$ sec for 82×42 grids. The time step is $\Delta t = 2.89 \times 10^{-7}$sec. Time-averaged data are created by averaging the flow field for sufficiently long time about 1×10^5 steps of unsteady flow simulations.

Flow Field Analysis

Computed results are shown for the entire flow field of shock wave turbulent boundary layer interaction in Fig 3. To explain the observed unsteady behaviour in the computational solution, the numerical scheme adopts may not guarantee monotone convergence, however, it will be analysed here. The unsteady observed might be due entirely to sources generated by the numerical scheme. The dominant frequencies do not exist in the unseparated case. Therefore, present numerical represents unsteady flow characteristics.

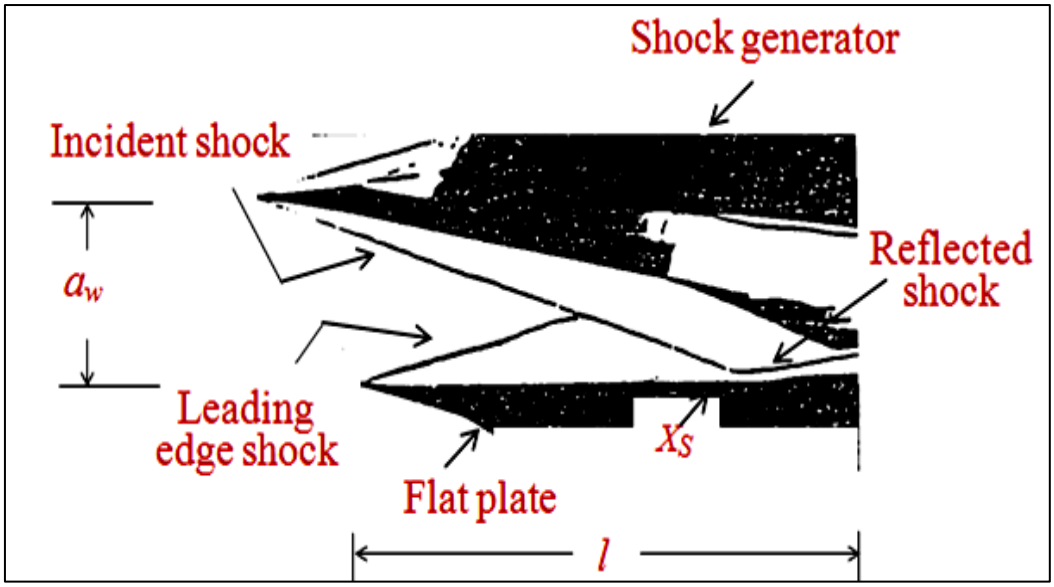

Fig 3: Schlieren picture of shock wave turbulent boundary layer interaction

Computed isobars contour plot is shown for the entire flow field of shock wave turbulent boundary layer interaction in Fig 3 for $Re_\infty = 72.8 \times 10^6$/m. Comparison is made between isobar contour plot with schlieren picture [11]. The contour picture reproduces all the essential features of Mach 6 interacting flow field as depicted in Fig 4 for various values of Reynolds number. From the contour plots, one can observe leading edge shock from the leading edge of the plate. The incident and reflected shock are also visible. The influence of Reynolds number on the on the reflected shock can be seen in Mach contour plots.

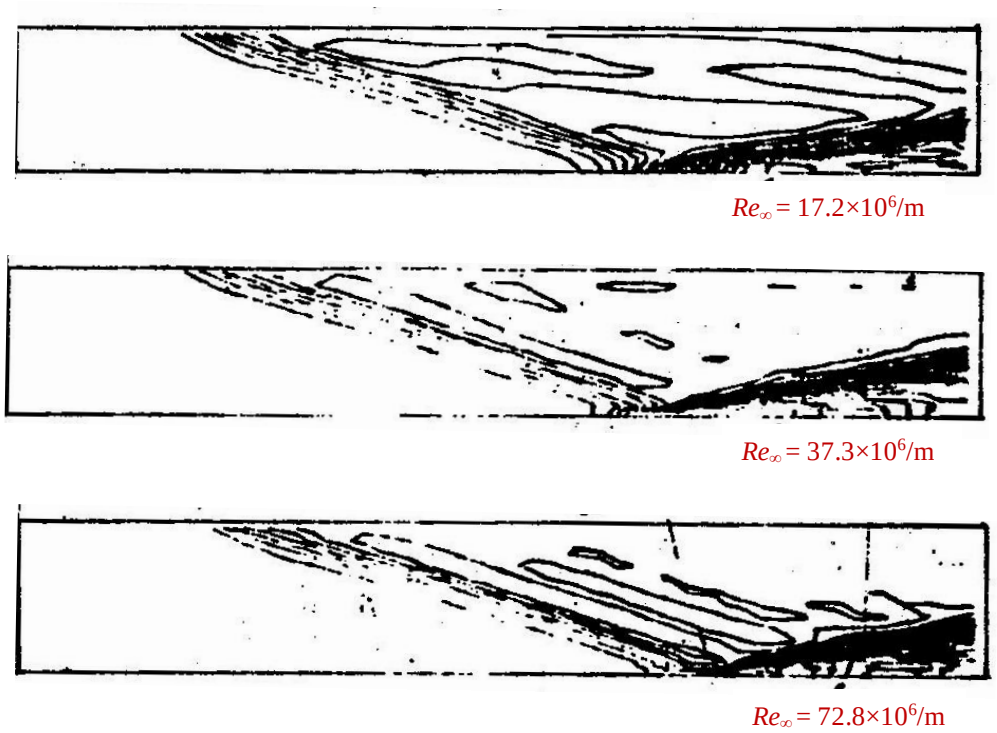

Fig 4: Mach contour plots of SWBLI for various values of Re_∞

The comparison of the pressure normalized by stagnation pressure (p/p_o) with the experimental data [11] is presented in Fig 5(a). The peak pressure associated with the impinging shock is found near to shock impingement point. Ahead of the separation bubble, a pressure plateau is seen that indicates the presence of a flow separation over the flat plate. The variation of heat transfer coefficient along flat plate surface is shown in Fig 5(b). The mean heat transfer coefficient increases after reattachment point. An agreement is seen between experimental data of [11] and present numerical results. Flow separation was noticed at

Re_∞ =37.3×10^6 and 72.8 ×10^6/m. the flow separation was also confirmed with experimental data as well as with axial velocity profiles in normal direction.

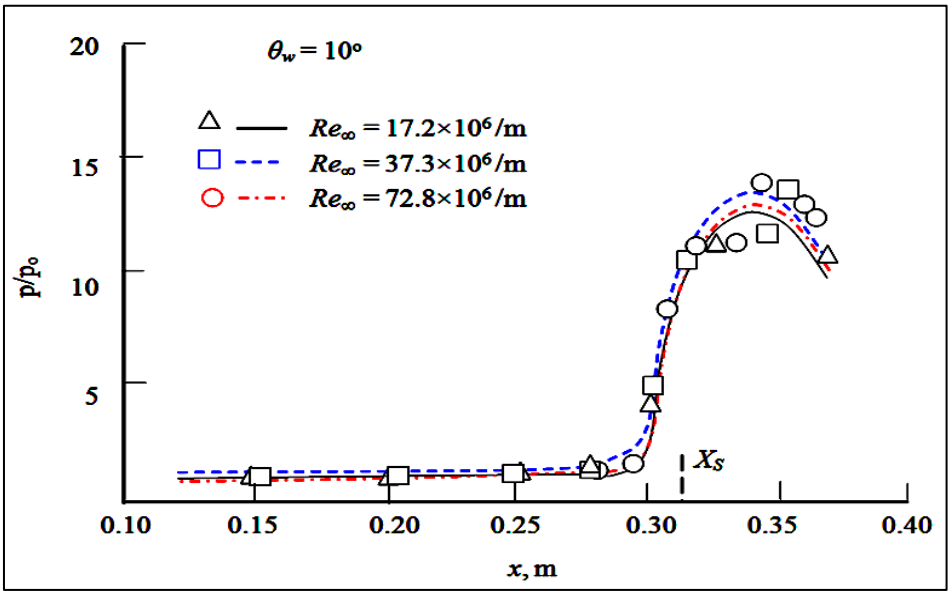

Fig. 5(a): Variation of surface pressure over a flat plate

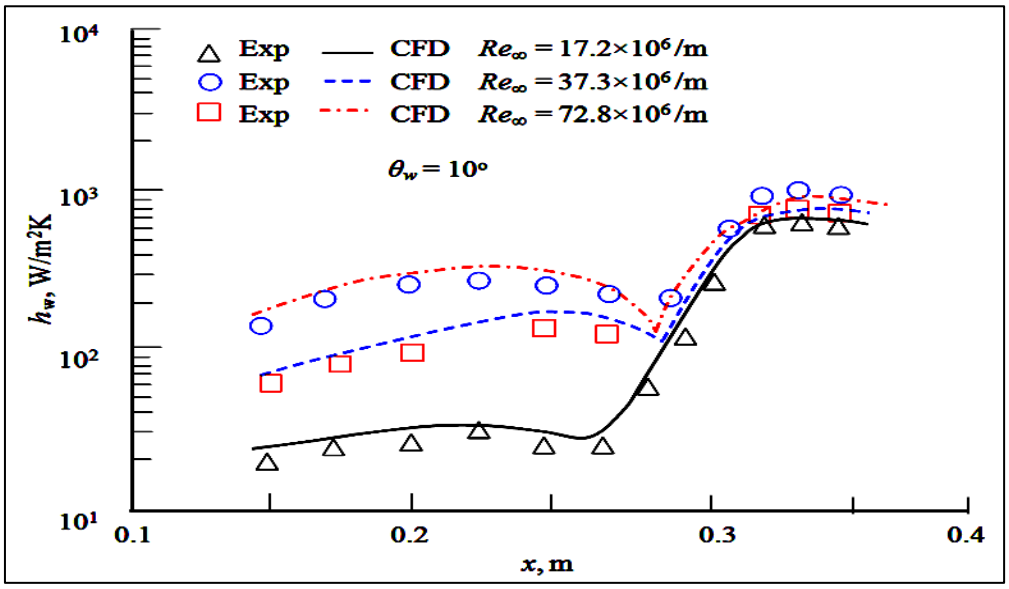

Fig 5(b): Variation of wall heat transfer coefficient over a flat plate

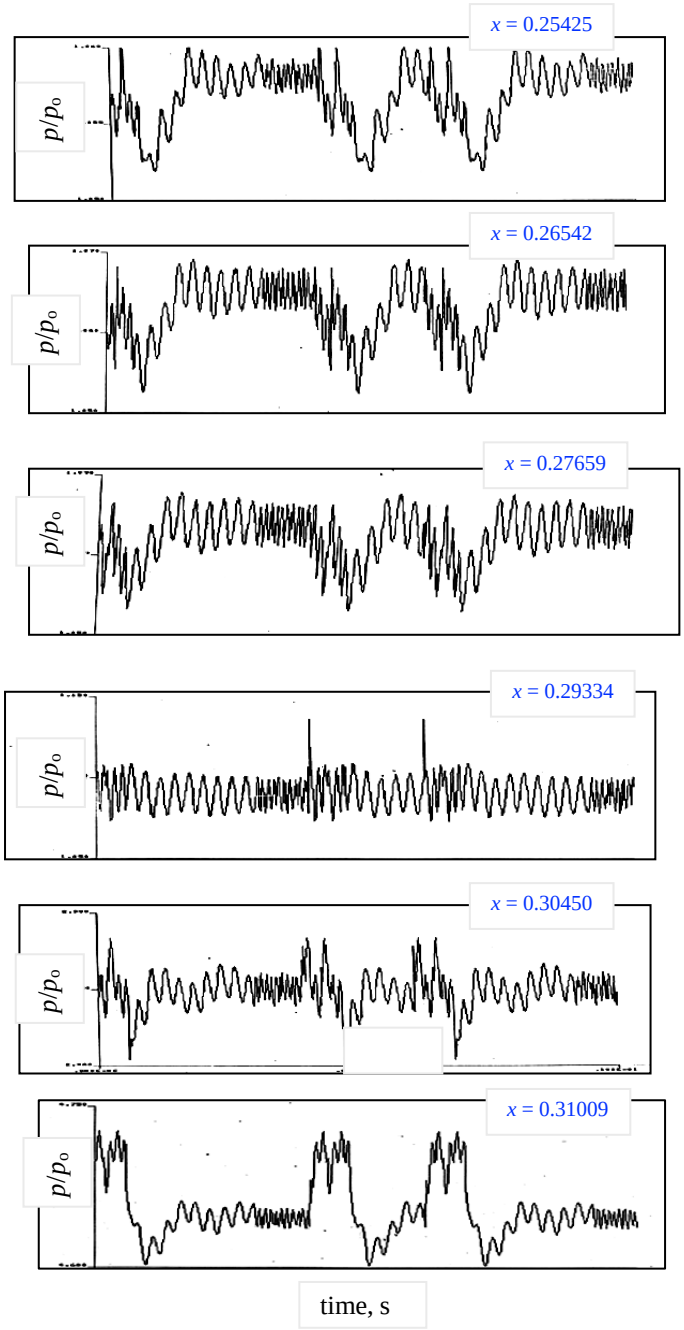

Fig 6: Wall pressure time history

Analysis of unsteady flow field data

The flat plate was discretized by 82 equally spaced grid points in axial direction. At each grid point, during computation a sufficient amount of time-dependent data was stored for unsteady analysis. Owing to the limited computational resources available, the spectral analysis is carried out in vicinity of the separation region. For $Re_\infty = 72.8 \times 10^6$/m.

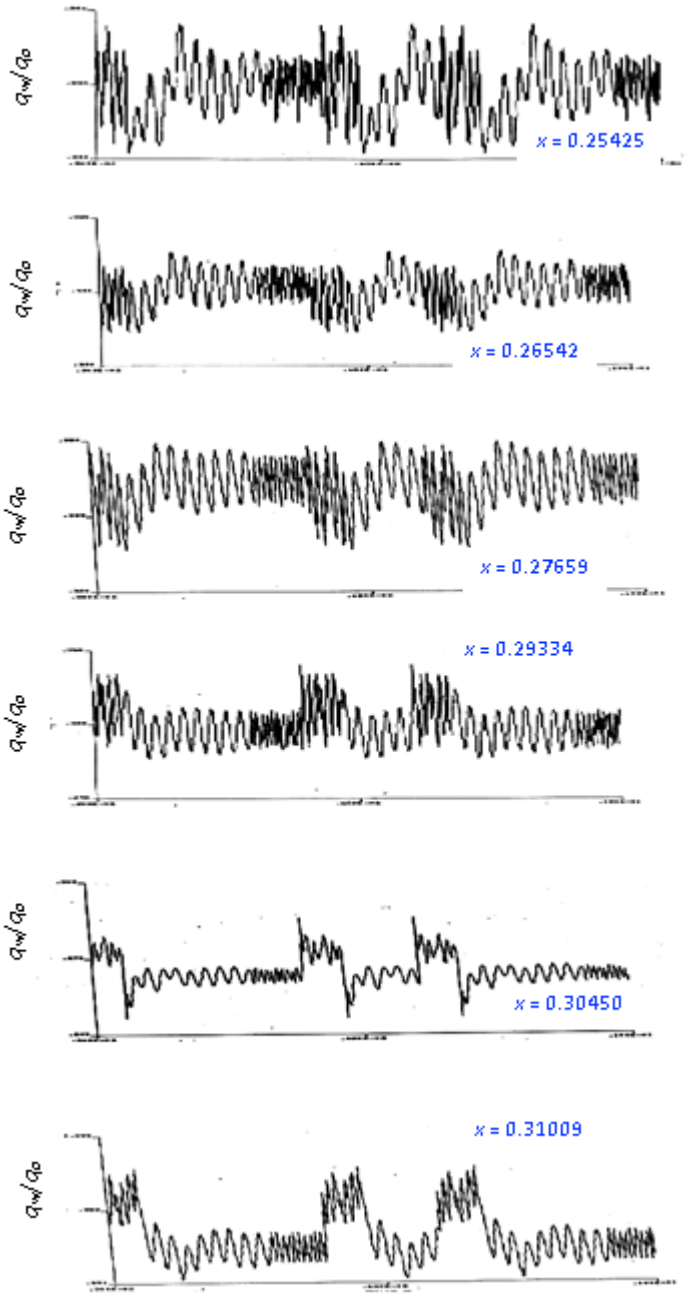

Fig 7: Wall heat flux time history

The sensitivity of pressure and heat transfer fluctuations at six sample stations near the separation point are used, viz., x = 0.25425, 0.26542, 0.27059, 0.29334, 0.30459 and 0.31009 m, where x is measured from the leading edge of the flat plate. The surface pressure (p/p_o) and the surface heat flux (q_w/q_o) variations at the aforementioned points are shown in Figs 6 and 7 as a function of time, where subscripts o and w represent stagnation and wall quantities, respectively. The scales are so selected as to emphasize the amplitude variations. It can be observed from the pressure and the heat flux time history that fluctuations in pressure and heat flux is manifested. Thus, the pressure and the heat flux data are from the transitional phase, i.e., the pressure and the heat flux values were really representative of the data, had the computation been continued for a very large time.

The analysis of the separated flow shows that the dominated frequency does not come into picture in the computation of pressure and heat flux quantities. This indicates a monotonic convergence of the numerical scheme.

A critical examination of the data points reveals that the secondary oscillations, through bounded, in the surface pressure and heat flux signatures cause only a slight increase at depicted in Figs 6 and 7. These fluctuations may be due to the numerical procedure or turbulent model. In practice such fluctuations arise from the nature of turbulence characteristics.

Spectral analysis of unsteady flow

Spectral analysis was carried out using Fast Fourier Transform FFT for all possible modes of fluctuations. The surface pressure and wall heat flux from time domain are changed into the frequency domain employing FFT, MATLAB® [12]. The surface pressure values have been transformed from pascal to SPL in decibels *dB*. The frequencies for which assessment was done were multiples of the fundamental frequency 121 Hz. The sound pressure level SPL were computed in terms of the pressure referenced at 20 μPa. Figures 8 and 9 present surface pressure and wall heat flux time history, respectively, at x = 0.25425 to 0.31009 m. A critical examination of the data points reveals in Figs 8 and 9 that the secondary fluctuations in the surface pressure and wall heat flux signature, though bounded, cause only a slightly increase. The scales are selected to emphasize the amplitude variations. It can be observed from the pressure and the heat flux time history that periodicity in pressure and heat flux is manifest. The pressure and the heat flux data are free from the transitional phase. The surface pressure and wall heat flux values were statically representative of the numerical data. The surface pressure and wall heat flux fluctuations show two major peaks. The oscillations in wall heat flux have qualitatively the same features as those of the wall pressure but differ quantitatively. Identical observations have been made in experiment by Hayashi *et al*., [1].

The global time step Δt is about 2.81×10^{-7} s. Time-averaged data are created by averaging the flow fields for sufficiently long time about 1.2×10^5 steps (34.7ms in physical time) of unsteady flow simulations.

Figures 8 and 9 show spectral analysis of surface pressure and wall heat flux fluctuations, respectively from x = 0.25425 to x = 0.31009 m. The spectral analysis of surface pressure and wall heat flux oscillations show two dominant frequencies, one at approximately 645 Hz and another one at approximately 5 kHz. Considering the 645 Hz signal, this appears to be roughly in phase across the region examined, i.e., x = 0.25425 to x = 0.31009 m. In the pressure-time history plots of Fig 6 two dominant frequencies can be observed, one at approximately 400 Hz and one at approximately 6 kHz. Considering the 400 kHz signal, this appears to be roughly in phase across the region examined (x = 0.25425 to x = 0.31009 m). The amplitude of the pressure fluctuations also appears to increase with axial distance x increasing. This is consistent with "*a solid body motion*" of the interaction region since the local amplitude would be a function of the slope of the pressure curve in Fig 5(a). However, the heat fluxes plotted in Fig 5(b). Prior to the separation point (or at least the maximum in heat region the heat flux should be in antiphase with the pressure. Beyond this point the slope is positive as we should see heat flux and pressure phase.

The spectral analysis of the pressure and the heat flux fluctuations shows two dominant frequencies, one at approximately 845 Hz and another one at about 6 kHz. The sound pressure level of the pressure fluctuations also increases as the axial distance x increases. The heat flux should therefore be in antiphase with pressure in this region. However, in the experiment conducted by Hayashi, Aso and Tan [1], it is shown that pressure and heat flux fluctuations are in the same phase throughout shock wave turbulent boundary layer interaction. Beyond this point, the slope is positive and pressure and heat flux fluctuations are in phase. The present numerical algorithm has simulated physical mechanism of unsteadiness at the reattachment point of shock separated high-speed flows. An intense heating rate was observed at the reattachment point. The sound pressure level SPL values are high and coupled with low frequency.

Hayashi, Aso and Tan [1] have obtained shock motion frequency at about 620 Hz at M_∞ = 4.0, T_w/T_∞ = 0.56, $Re_{x,s} = 12.6 \times 10^6$, and $\theta_w = 18.5^o$. $Re_{x,s}$ represent Reynolds number at the shock impingement point as depicted in Fig 2. The mean teat transfer distribution increases after the reattachment point. The wall pressure and the heat flux fluctuations show two peaks. From a comparison of pressure and heat flux fluctuations, in heat flux quantitatively the same features as those of the wall pressure fluctuations but have noticeable quantitative differences. Identical observations have been made in experiment by Hayashi, Aso and Tan [13]. When the boundary layer separates, significant fluctuations of heat flux exist in the entire region of shock wave turbulent boundary layer interaction.

Physically, one mechanism for the unsteadiness observed in supersonic separated flows is ascribed in pressure fluctuations at reattachment. The source of any such disturbance, should they be due to physical phenomena, must therefore be ascribed to attributes of the flow which the code can model.

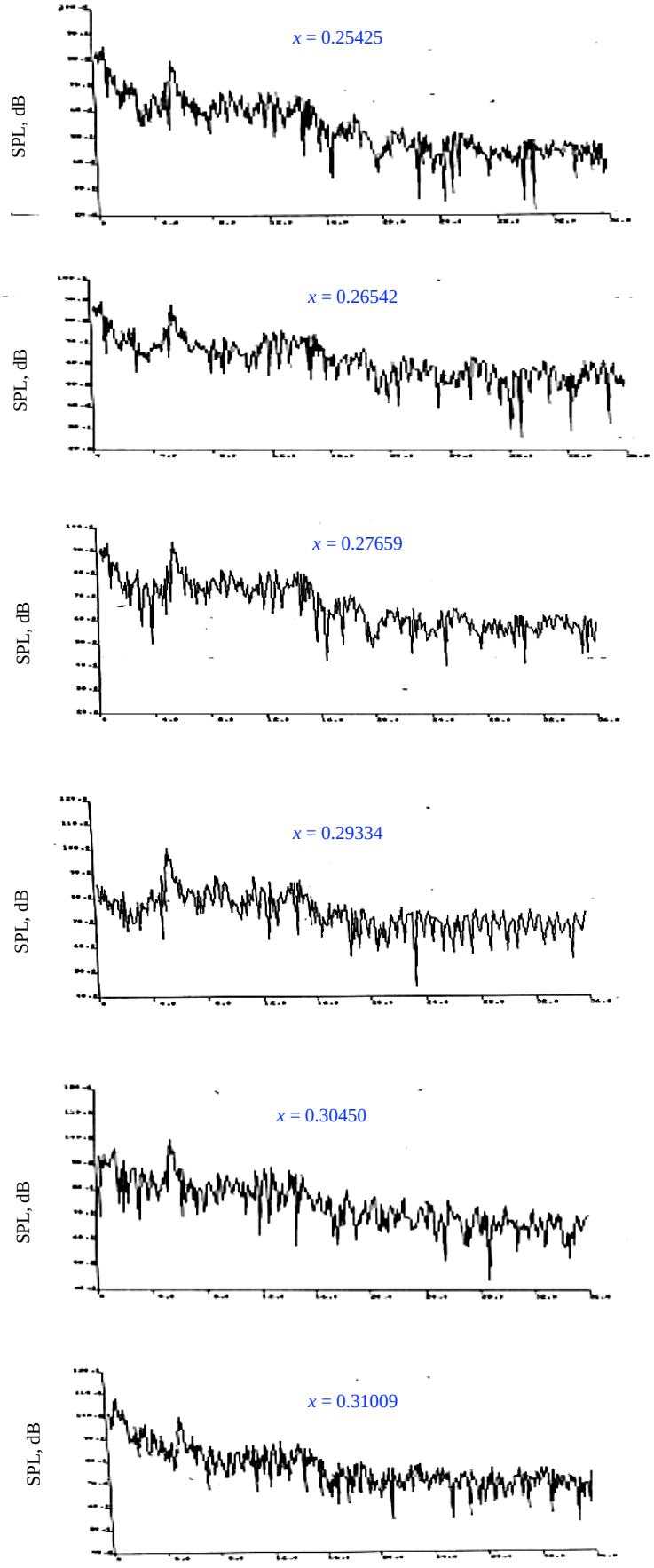

Fig 8: Spectral analysis of pressure fluctuations

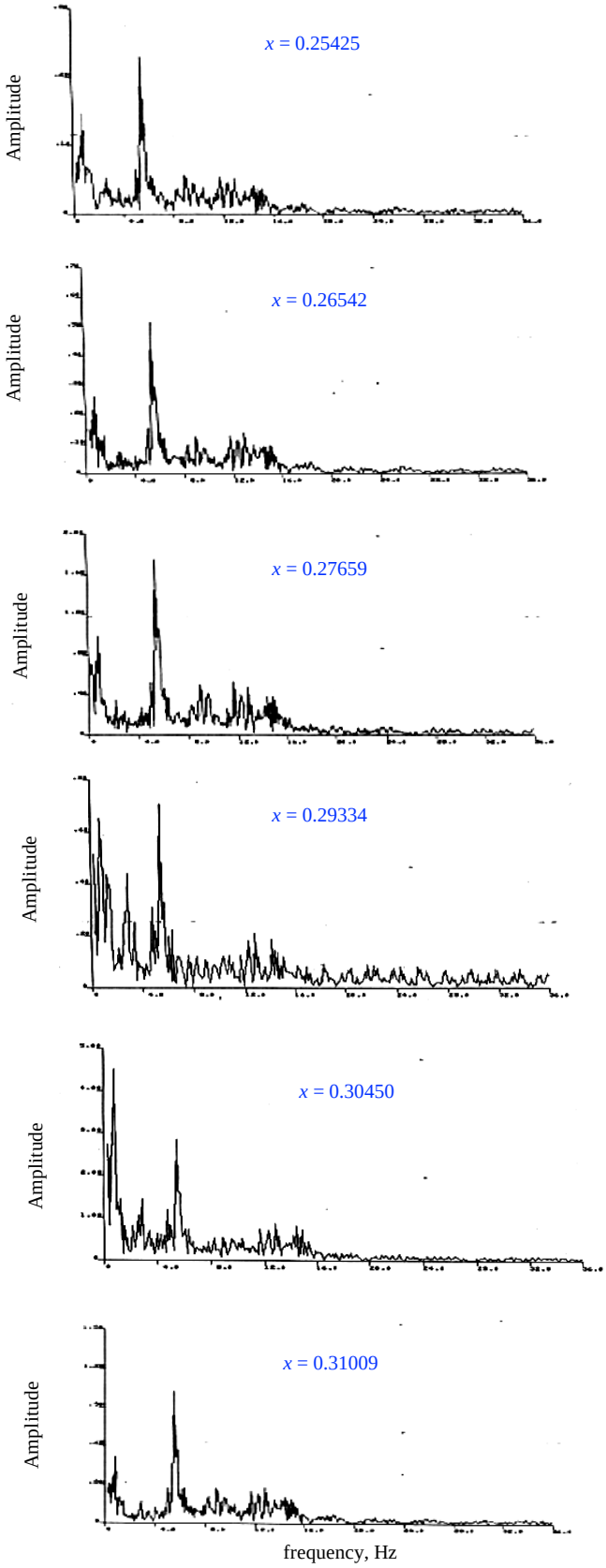

Fig 9: Spectral analysis of heat flux fluctuations

The surface pressure distributions have shown that the comparable intermittency in the same region, and the disturbed levels appear with the about same frequency at the same point. The intermittent phenomena attributed to the shock system fluctuations. Present numerical simulation shows a low-frequency

unsteadiness at separation and a high-frequency at reattachment due to shock wave turbulent boundary layer interaction as observed by Gross *et al*., [8].

Hankey and Holden [14], Dolling and Murphy [15] and Viswanath [16] pointed that the intermittent is a feature of the separated interactions between shock wave turbulent boundary layer interaction. A transient thin-wall technique [17] can be used to measure temperature-time history in to compare the present numerical analysis.

The acoustic level near the separation point is about 110 dB which is comparable to our numerical simulation on a bulbous heat shield. However, experimental studies are required to validate it. A critical examination of the data points reveals that the secondary oscillations, through bounded, in the surface pressure and heat flux signifies cause only a slightly increase.

4. CONCLUSIONS

Unsteadiness of the flow field is numerically analysed at $M_\infty = 6$, $\theta_w = 10^o$, $T_w/T_\infty = 0.56$ and Re_∞ =17.2 × 10^6/m, 37.3 × 10^6/m, 72.8 × 10^6/m. This Reynolds number range will produce without separation, minor separation, and significant amount of separation induced by an impinging oblique shock on a flat plate. All the essential flow features are captured well in the numerical simulations. The computed data for mean surface pressure and mean wall heat transfer coefficient has shown a good agreement with available wind-tunnel data. Spectral analysis is carried out using FFT. The maximum shock wave frequency is about 645 Hz. The maximum SPL of 110 dB is found near the separation points.

REFERENCES

1. Hayashi, M., Aso, S., & Tan, A. (1989). Fluctuation of heat transfer in shock wave/turbulent boundary layer interaction. *AIAA Journal*, *27*(4), 399-404.
2. Dolling, D. S. (2001). Fifty years of shock wave/turbulent boundary layer interaction research what next. *AIAAJ*, *39*(8), 1517-1531.
3. Gaitonde, D. V. (2005). Progress in shock wave/turbulent boundary layer interactions. *Progress in Aerospace Sciences*, 72, 80-99.
4. Delery, J., & Dussauge, J. P. (2009). Some physical aspects of shock wave/turbulent boundary layer interactions. *Shock Waves*, 19, 453-468.
5. Clemens, N. T., & Narayanaswamy, V. (2014). Low-Frequency unsteadiness of shock wave/turbulent boundary layer interactions. *Annual Review of Fluid Mechanics*, 46, 469-492.
6. Lu, X. G., Yi, S. H., He, L., Liu, X. L., & Zhang, F. (2020). Experimental study on time evolution of shock wave and turbulent boundary layer interactions. *Journal of Applied Fluid Mechanics*, *14*(6), 1769-1780.
7. Tong, F., Ji, X., Deng, S., Yuan, X., & Li, X. (2024). On turbulent heat flux and temperature variance in supersonic shock wave and turbulent boundary layer interactions, Computer & Fluids, 2024.
8. Gross, A., Little, J. C., & Fasel, H. F. (2018). Numerical investigation of shock turbulent boundary layer interaction, AIAA 2018-1807.
9. MacCormack, R. W. (1981). Numerical methods for compressible flow, Workshop-cum-Seminar on Compressible Fluid Dynamics, held on at Vikram Sarabhai space Centre, Trivandrum, India, Dec. 14-21.
10. Baldwin, B. S., & Lomax, H. (1978). Thin layer approximation and algebraic model for separated turbulent flows, AIAA paper 78-257.
11. Johnson, C. B., & Kaufman, II, L. G. (1974). Interference heating from interaction of shocks with turbulent boundary layers at Mach 6, NASA TN-D 7649.
12. MATLAB User's Guide, The MathWorks, Inc. USA, July 2020.
13. Hayashi, M., Aso, S., & Tan, A. (1987). Unsteady aerodynamic heating phenomena in the interaction of shock wave/turbulent boundary layer, Memorial of the Faculty of Engineering, Kyushu University, 47(4) December 1987.
14. Hankey, W. L., & Holden, M. S. (1975). Two-dimensional shock wave boundary layer interactions in high speed flows, AGRDograph 203.
15. Dolling, D. S., & Murphy, M. T. (1983). Unsteadiness of the separation shock wave structure in a supersonic compressible ramp flow field. *AIAA Journal*, *21*(12), 1628-1634.
16. Viswanath, P. R. (1988). Shock-wave-turbulent-boundary-layer interaction and its control, Sadhana, Vol. 12, Parts 1 & 2, 45-104.
17. Nicoll, K. M. (1963). Use of Transient "Thin-Wall" Technique in Measuring Heat Transfer Rates in Hypersonic Separated Flows. *AIAA journal*, ***1***(4), 940-941.